PHOTONICS Research

# Mode demultiplexing hybrids for mode-division multiplexing coherent receivers

He Wen,[1,*] Huiyuan Liu,[1] Yuanhang Zhang,[1] Peng Zhang,[1,2] and Guifang Li[1,3]

[1]CREOL, The College of Optics & Photonics, University of Central Florida, Orlando, Florida 32816-2700, USA
[2]Changchun University of Science and Technology, Changchun 130012, China
[3]e-mail: li@ucf.edu
*Corresponding author: he.wen@creol.ucf.edu

Received 25 February 2019; revised 8 May 2019; accepted 7 June 2019; posted 10 June 2019 (Doc. ID 360809); published 29 July 2019

**We propose a mode demultiplexing hybrid (MDH) that integrates mode demultiplexing, local oscillator power splitting, and optical 90-deg mixing using multi-plane light conversion (MPLC). We demonstrate the realization of a three-mode MDH using four phase plates, one more than what is required for an MPLC-based mode demultiplexer, via numerical simulations. The performance of the three-mode MDH is comparable to that of commercial single-mode 90-deg hybrids. This multiple-functionality device enables simplification of the coherent optical front end of mode-division multiplexing receivers.** 

https://doi.org/10.1364/PRJ.7.000917

## 1. INTRODUCTION

Space-division multiplexing (SDM), which utilizes the spatial domain as a new physical dimension for communication, has been explored to increase the fiber-optic transmission capacity by overcoming the nonlinear Shannon capacity limit imposed by fiber nonlinear effects [1–3]. Many researchers have demonstrated, either theoretically or experimentally, that employing spatial modes as well as fiber cores can significantly increase system capacity [4–8] and/or spectral efficiency [6], improve system performance [9–11], or reduce system cost [12,13]. To fully compensate for the linear impairments to the signal from transmission, coherent detection and digital signal processing are employed to retrieve both signal amplitude and phase [14]. The coherent optical front end for a mode-division multiplexing (MDM) receiver consists of a mode demultiplexer and an optical 90-deg hybrid for each mode [15]. The mode demultiplexer separates all $M$ spatial modes and converts them to the fundamental mode at different positions. An optical 90-deg hybrid mixes each demultiplexed mode with a local oscillator (LO) to extract the in-phase and quadrature components of the signal. The number of required optical 90-deg hybrids is equal to the number of mode channels. For wavelength-division multiplexed (WDM) systems with $N$ wavelength channels [16], the required number of optical 90-deg hybrids is $M \times N$ (for single polarization; it is doubled for polarization multiplexing). These hybrids occupy a large footprint and make the receivers complicated. Fortunately, current integration technique allows the optical 90-deg hybrid to be integrated with the balanced photodetector to reduce the overall footprint [17]. However, active control of phase retardation in the optical 90-deg hybrid is generally required [18], which increases system power consumption.

In this paper, we propose a single device called the mode demultiplexing hybrid (MDH) to simultaneously realize mode demultiplexing and optical 90-deg mixing using multiplane light conversion (MPLC), which will simplify the structure of the coherent optical front end. With a broad bandwidth, the MDH operates across multiple wavelength-MDM channels; therefore; the mode demultiplexer and the $M \times N$ optical 90-deg hybrids can be replaced by a single MDH. Furthermore, the stable 90-deg phase retardation offered by the MDH eliminates the need for phase stabilization, in contrast to waveguide-based optical 90-deg hybrids, resulting in power savings. The underlying principle for the versatile functionality of an MDH is that arbitrary unitary transforms can be realized by MPLC [19]. Since the operations of mode-demultiplexing, power splitting, and the 90-deg hybrid are all unitary transforms, they can be lumped together as a composite unitary transform and realized by MPLC.

This paper is organized as follows. Section 2 introduces the principle behind MPLC to construct optical components, such as interferometers, optical 90-deg hybrids, and mode demultiplexers, and shows how to build an MDH through the combination of interferometers and a mode demultiplexer. In Section 3, we present simulation results for an MDH for three linearly polarized (LP) modes. Section 4 is the conclusion.

## 2. PRINCIPLE OF MPLC-BASED OPTICAL 90-DEG HYBRIDS

MPLC is a class of systematic implementation of arbitrary unitary transform in practice, which is used to construct various

functional devices. MPLC is composed of a sequence of phase modulations followed by a fixed linear transformation such as an optical Fourier transform or Fresnel transform. With a sufficient number of phase modulations, MPLC approaches an arbitrary unitary transform with an error smaller than a desired value. MPLC is very useful in optics because a simple input beam can be losslessly converted into a beam with a complex profile. If the input beams are orthogonal (zero overlap integral in the transverse plane), the outgoing beams are also orthogonal. There are two common forms of orthogonality. One occurs when the input beams have no spatial overlap. The other occurs when the input beams are spatially overlapped but with different symmetries. Physically, MPLC can be realized through a series of phase plates and on-axis lenses separated by a focal length or a reflective cavity where the phase plates are carved onto one end of the cavity [20]. MPLC has been shown to have applications in quantum optics as mode sorters [21] and in classical optical fiber communications as mode multiplexers (MUXs)/demultiplexers (DeMUXs) [20]. MPLC has been used to sort as many as 325 modes [21]. It is worth noting that in these applications, MPLC was only used to convert one beam to another beam without other signal processing abilities.

To realize effective signal processing, we need to split the input signals into many copies and combine them with a desired set of weighted coefficients. MPLC inherently possesses this required capability because optical beams in MPLC propagate mostly in free space. First, MPLC can easily split one beam into a set of beams or spatially overlap beams with gratings on phase planes. Second, orthogonality between beams is defined over the entire spatial domain and is generally not preserved over a part of the original spatial domain. As a result, different combining coefficients can be realized by integrating over different sections of the spatial domain. Third, in contrast to waveguide-based interconnect devices (e.g., interferometers), it is easier for MPLC to realize the cross-connects and interconnects of multiple input beams to facilitate signal processing, because optical beams in MPLC propagate mostly in free space. Not confined in waveguides, MPLC-based cross-connects and interconnects are less affected by environmental perturbations such as temperature drift and vibration. The high stability of MPLC is achieved at the cost of lack of flexibility, such as tunability of the power splitting ratio and operating wavelength. However, in some devices, such as optical 90-deg hybrids, stability is more important than flexibility. In what follows, we explain how to construct MDHs through a few simple examples.

### A. MPLC-Based Interferometers

Let us start with the well-known mode multiplexer. In this multiplexer, there are two coherent input beams in the fundamental Gaussian mode located in different positions with zero spatial overlap shown in Fig. 1(a). MPLC can convert the two beams into two overlapped and orthogonal beams, one in the linearly polarized (LP) $LP_{01}$ mode and another in the $LP_{11}$ even mode, by diffracting the beams with different input patterns on the same phase plates. We note that the two lobes of the $LP_{11e}$ mode are out of phase with equal power. If we treat the overlapped fields of the $LP_{01}$ mode with the upper and lower lobe in the $LP_{11e}$ mode as two separate outputs, they are simply the outputs of a two-port interferometer as shown in Fig. 1(b) and as given by Eq. (1) as follows:

$$\begin{aligned} P_{o1} &\propto \iint_{y>0} |A_{01}\Phi_{01}(x,y) + A_{11}\Phi_{11}(x,y)\exp(i\theta)|^2 \mathrm{d}x\mathrm{d}y \\ &= |A_{01}|^2 \iint_{y>0} \Phi_{01}^2(x,y)\mathrm{d}x\mathrm{d}y + |A_{11}|^2 \iint_{y>0} \Phi_{11}^2(x,y)\mathrm{d}x\mathrm{d}y \\ &\quad + 2\mathrm{Re}(A_{01}A_{11}^*) \iint_{y>0} \Phi_{01}(x,y)\Phi_{11}(x,y)\mathrm{d}x\mathrm{d}y\cos\theta \\ &= \frac{1}{2}(P_{01}+P_{11}) + \sqrt{P_{01}P_{11}}\eta\cos\theta, \\ P_{o2} &\propto \iint_{y<0} |A_{01}\Phi_{01}(x,y) - A_{11}\Phi_{11}(x,y)\exp(i\theta)|^2 \mathrm{d}x\mathrm{d}y \\ &= \frac{1}{2}(P_{01}+P_{11}) - \sqrt{P_{01}P_{11}}\eta\cos\theta. \end{aligned} \tag{1}$$

Here $A_{00}$, $A_{10}$, $\Phi_{00}$, and $\Phi_{10}$ are the amplitudes and transverse beam profiles of the $LP_{01}$ and $LP_{11}$ modes, respectively; $\theta$ is the phase retardation difference between the input beams; $\eta$ is the coupling efficiency for one lobe, defined as

$$\eta = \iint_{y>0} \Phi_{01}\Phi_{11}\mathrm{d}x\mathrm{d}y \Big/ \sqrt{\iint_{y>0} \Phi_{01}^2\mathrm{d}x\mathrm{d}y \iint_{y>0} \Phi_{11}^2\mathrm{d}x\mathrm{d}y}. \tag{2}$$

Note the area of integration is over the upper half plane (vertical position $y > 0$), not the entire plane (for which $\eta$ becomes

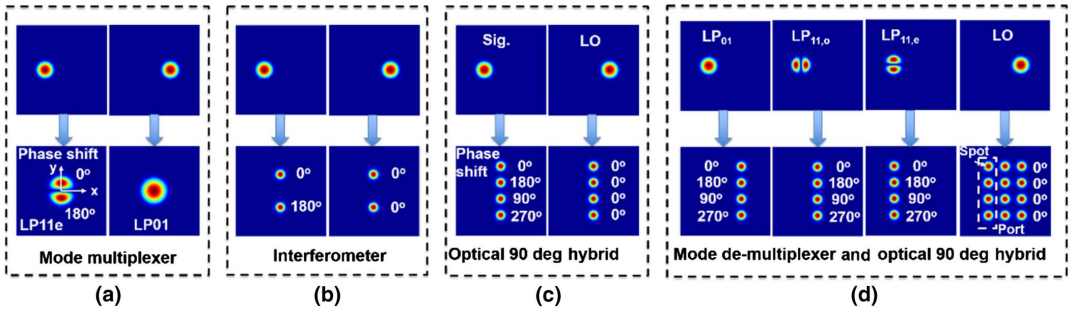


**Fig. 1.** Illustration of input-to-output mapping for MPLC-based devices. (a) Mode multiplexer converting two separated input beams into two overlapped orthogonal beams; (b) interferometrically combining two separated input beams; (c) optical 90-deg hybrid mixing of two separated input beams; (d) mode demultiplexer and optical 90-deg hybrid separating and converting orthogonal overlapped modes and mixing with their respective local oscillators. The phase retardations of the spots are marked alongside them.

zero). We utilize the even and odd symmetry of the $LP_{01}$ and $LP_{11}$ mode to obtain Eqs. (1) and (2).

The two lobes of the converted $LP_{11}$ mode do not necessarily have to be close together; they can be separated far apart and have the same spatial distributions as the fundamental mode as shown in Fig. 1(b). We will call these separated components spots hereafter. Essentially, the first input Gaussian beam can be converted into two spatially separated, out-of-phase spots by an MPLC. Similarly, the second input Gaussian beam is converted by the same MPLC into two spatially separated, in-phase spots overlapped with the two spots from the first Gaussian beam as shown in Fig. 1(b). An MPLC can implement such a conversion because the output beams (comprising multiple spots) remain orthogonal. Such an MPLC performs the function of a symmetric optical interferometer.

### B. MPLC-Based Optical 90-deg Hybrids

To realize an optical 90-deg hybrid, we need two symmetric interferometers having a phase offset difference of 90 deg between each other. This can be accomplished using an MPLC. In Fig. 1(c), we convert each of the input beams, representing the signal and the LO, into four separate spots, the profiles of which are all the same. To make this conversion feasible, the output beams must be orthogonal. One of the possible solutions is to make the pair-wise differences in phase retardation between the four spots from the two input beams as 0, $\pi$, $\pi/2$, and $-\pi/2$ so that

$$\begin{aligned}\iint E_1 E_2^* \mathrm{d}x\mathrm{d}y &= A_1 A_2^* \exp(i\theta) \\ &\times \left[\iint_{S_1} \Phi^2 \mathrm{d}x\mathrm{d}y + \iint_{S_2} \Phi^2 \mathrm{d}x\mathrm{d}y \exp(i\pi)\right. \\ &\left. + \iint_{S_3} \Phi^2 \mathrm{d}x\mathrm{d}y \exp\left(i\frac{\pi}{2}\right) + \iint_{S_4} \Phi^2 \mathrm{d}x\mathrm{d}y \exp\left(-i\frac{\pi}{2}\right)\right] = 0,\end{aligned} \tag{3}$$

and therefore the output beams remain orthogonal. The subscript $S_i$ ($i = 1, 2, 3, 4$) denotes the integral area of spot $i$. The optical powers of the four separated spots in the same group are

$$\begin{bmatrix} P_{o1} \\ P_{o2} \\ P_{o3} \\ P_{o4} \end{bmatrix} = \frac{1}{4}(P_1 + P_2) + \frac{1}{2}\sqrt{P_1 P_2} \begin{bmatrix} \cos\theta \\ -\cos\theta \\ \sin\theta \\ -\sin\theta \end{bmatrix}. \tag{4}$$

They are exactly the outputs of a standard optical 90-deg hybrid, containing the in-phase and quadrature components of the signal projected onto an LO. Balanced detections $P_{o1} - P_{o2}$ and $P_{o3} - P_{o4}$ can be used to suppress the unwanted DC component $(P_1 + P_2)/4$, where $P_1$ and $P_2$ are the input beam power.

It is worth noting that the phase retardations introduced by the MPLC are very stable for two reasons. (1) Unlike waveguides, the dominant free-space light paths in MPLC are not affected by environmental perturbations. The phase plates are thin and therefore with negligible influence of environmental variations. (2) One pixel-induced phase retardation deviation in a previous phase plate will spread to all pixels in the next phase plate due to diffraction. A manifestation of this tolerance of MPLC is the fact that the quantized phase retardation provided by gray-scale lithography [20,22] can generate desired beams with high quality, where the generated high-order modes, which contain phase retardation in adjacent lobes, are highly stable. Consequently, the phase retardation offered by MDH does not require stabilization control, which is often needed in waveguide based devices.

### C. Mode-Demultiplexing Optical 90-deg Hybrids

This optical 90-deg hybrid working for the fundamental mode can be generalized to a mode demultiplexing hybrid as shown in Fig. 1(d). The input beams are $M$ spatially overlapped orthogonal modes. The input beams are converted into non-overlapped beams, each composed of four spots with phase retardations of 0, $\pi/2$, $\pi$, and $-\pi/2$. The LO is split into $M$ groups, each having four spots with the same phase retardation. Each group of spots from the LO is overlapped with the group of spots of the demultiplexed mode at the output port [marked by a dashed rectangle in Fig. 1(d)]. In such a configuration, a device that performs both mode demultiplexing and multichannel optical 90-deg hybrid is realized. The required number of phase plates for the MDH is one more than that for the same mode demultiplexer. Generally, the number of phase plates for the mode demultiplexer is determined by the number of independent modes. The extra phase plate in the MDH is required for power splitting of the LO. The simple structure of the MDH benefits from the complex cross-connects and interconnects enabled by the beam splitting and combining in free space, without the constraints of waveguides.

In contrast, waveguide-based optical 90-deg hybrids only work well for single-mode inputs (fundamental mode in most cases). This is because different modes have different effective indices, resulting in different splitting ratios and different interferometric phase offsets.

Not limited to the LP mode bases, MDHs are applicable to other mode bases, such as orbit angular momentum (OAM) modes and Hermite–Gaussian modes. For any mode base, there is no information loss in this transformation process. Any mode crosstalk coming from random mode coupling in transmission or imperfect mode demultiplexing can be removed by processing the received signal with multiple-input and multiple-output (MIMO), which only requires that the overall transfer function is unitary.

## 3. SIMULATION VERIFICATION

We performed simulations to verify the proposed MDH concept. Assuming three input modes $LP_{01}$, $LP_{11,o}$, and $LP_{11,e}$ shown in Fig. 1(d), the three modes are demultiplexed and projected to three separate groups of four spots with phase retardations of 0, $\pi$, $\pi/2$, and $-\pi/2$, respectively. The LO is split and projected onto 12 in-phase spots. Four phase plates with $201 \times 201$ pixels were used in our simulations. The input $LP_{01}$ mode with a mode-field diameter of 228 μm propagated 3 cm in free space and arrived at the first phase plate with a mode-field diameter of 346 μm. The mode-field diameter of the output spots was 135 μm; the distance between adjacent spots was 255 μm. The pixel size of the phase plates was 6.8 μm. All

beams were normal to the phase plates to maintain the paraxial condition.

We used the wavefront-matching algorithm [23] coded in MATLAB to solve for the desired phase pattern of each phase plate. The algorithm updates the phase pattern by performing the overlap between the forward and backward propagating fields at the target plate plane iteratively until a stable result is reached. The unitary transform for free-space propagation between successive phase plates is modeled as Fresnel diffraction, in which the quadratic wavefront distortion in the transverse direction is considered.

Figure 2 shows the profiles of the four phase plates designed for the MDH and the beam intensity profiles right after each phase plate. The maximum intensity in each frame is normalized to one. Four phase plates are sufficient to effectively convert the three modes to the desired profiles at the designated positions, though a small portion of the input power is lost in the form of stray light and there exists a power imbalance between the spots. As the fourth phase plate is also the exit plane of the MDH, the phase pattern resembles the $4 \times 3$ spots array, because only the areas that coincide with the output spots can affect the output. The output $4 \times 3$ spot array contains the mixed LP modes and LO and can be directly detected without any external mixers.

In Fig. 3, we plot the amplitude and phase of the four output spots for the signal and LO along the central line in Fig. 3. The total output power of the four spots is normalized. The LO and signal fields are well aligned. The phase retardations of the four output spots match the desired ones except for some minor ripples. The unequal amplitudes of the four spots indicate that the input power is not equally divided. This is due to a finite number of phase plates being used. Increasing the number of phase plates can alleviate this power imbalance.

To evaluate the performance of the MDH quantitatively, we calculate the intra-port power uniformity, which we define as the ratio of the maximum to the minimum power of the four spots at output port $k$ (corresponding to mode $k$) $\Delta \mathrm{IL}_k = \max_{i\in\{1,2,3,4\}} P_{k,i} / \min_{i\in\{1,2,3,4\}} P_{k,i}$ and the phase retardation deviation, defined as the difference between the ideal 90-deg difference between the in-phase and quadrature component and the simulated phase retardation difference

$$\Delta\theta_k = \arg\left(\iint_{S_{k,3}} A_k\Phi_k \mathrm{d}x\mathrm{d}y - \iint_{S_{k,4}} A_k\Phi_k \mathrm{d}x\mathrm{d}y\right) - \arg\left(\iint_{S_{k,1}} A_k\Phi_k \mathrm{d}x\mathrm{d}y - \iint_{S_{k,2}} A_k\Phi_k \mathrm{d}x\mathrm{d}y\right) - \pi/2, \quad (5)$$

where $P_{k,i}$ is the power of spot $i$ at the output port for mode $k$, $S_{k,i}$ is the integrated area of spot $i$ at mode $k$ output, and $A_k$ and $\Phi_k$ are the complex amplitude and profile of the beam projected into port $k$. For the LO, the phase retardation deviation is defined as the maximum absolute phase difference of each spot from the average as

$$\Delta\theta_{\mathrm{LO}} = \max_{\substack{k\in\{1,\ldots,M\}\\ i\in\{1,2,3,4\}}} \left| \arg\left(\iint_{S_{k,i}} A_i\Phi_i \mathrm{d}x\mathrm{d}y\right) - \frac{1}{4M}\sum_k\sum_i \arg\left(\iint_{S_{k,i}} A_i\Phi_i \mathrm{d}x\mathrm{d}y\right)\right|. \quad (6)$$

In addition, we estimate the insertion loss (IL) for each mode and modal crosstalk by calculating the cross-correlation matrix with matrix elements as follows:

$$c_{k,l} = \left| \iint (\overline{A}_k\Phi_k)(\overline{A}_{l0}^*\Phi_{l0}) \mathrm{d}x\mathrm{d}y \right|, \quad (7)$$

which is the correlation between the normalized output field for mode $k$ and the desired output field for mode $l$. The

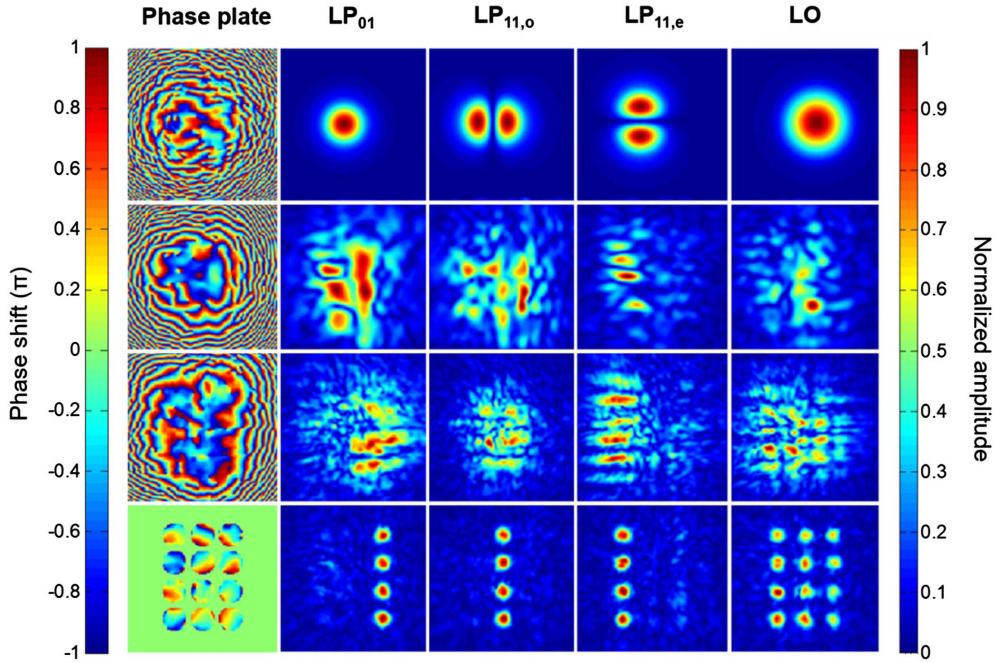


**Fig. 2.** Phase patterns of the designed phase plates and simulated beam intensity profiles right after each phase plate.

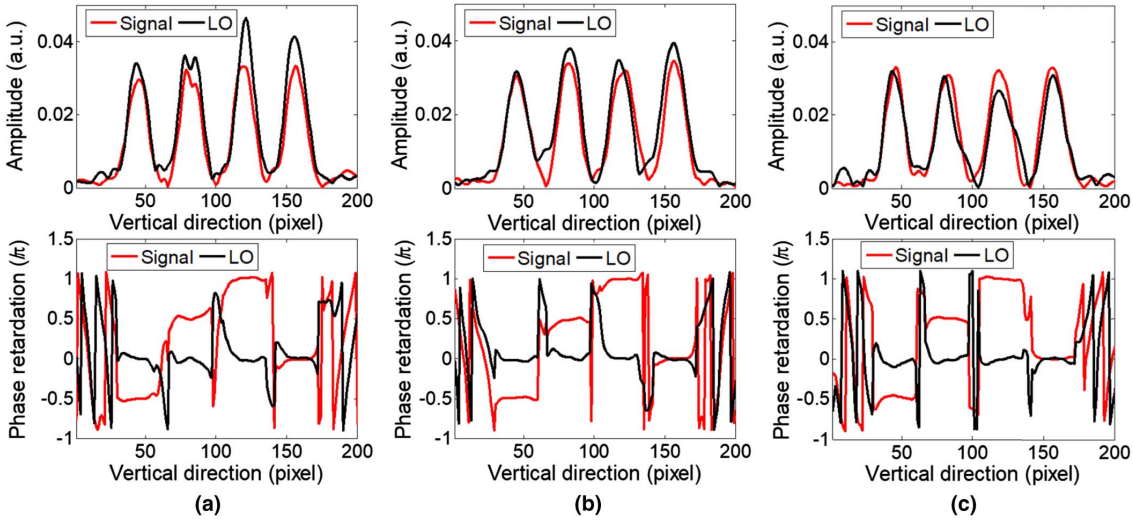


**Fig. 3.** Amplitude and phase retardation of output beam slice along the mirror symmetric line for the (a) $LP_{11e}$ mode, (b) $LP_{11o}$ mode, (c) $LP_{01}$ mode, and the LO.

cross-correlation matrix is shown in Fig. 4. The diagonal elements, representing the fidelity between the generated and desired output field, have a minimum value of 0.86 (−0.6 dB). The off-diagonal elements, characterizing the field crosstalk between different modes, have a maximum value of 0.05 (−13.0 dB). For coherent detection, field crosstalk is more meaningful than power crosstalk. Using singular-value decomposition, we factorize the correlation matrix uniquely as product of three matrices: a left unitary matrix, a diagonal matrix, and a right unitary matrix. The elements of the diagonal matrix are the four singular values $\lambda_k$ of the correlation matrix and equal 0.9630, 0.8743, 0.8672, and 0.8343. The mode-dependent insertion loss (MDL) is $10\log(\lambda_{\max}^2/\lambda_{\min}^2) = 1.25$ dB, and the average insertion loss is $10\log\sum_k\lambda_k^2/M = -1.08$ dB, excluding the 6-dB splitting loss. The results indicate a good performance of the MDH.

Next, we examine the photocurrent as a function of the phase shift of the input modes, relative to that of LO, with ideal balanced photodetectors. All three modes are injected into the MDH together with equal power. The power of each mode is one tenth the LO power after splitting. Therefore, both mode crosstalk and LO impairments, such as non-uniform splitting and phase retardation deviations, produce distortions in the photocurrents, which are shown in Fig. 5(a). The distortions approximately follow cosine and sine functions with a DC

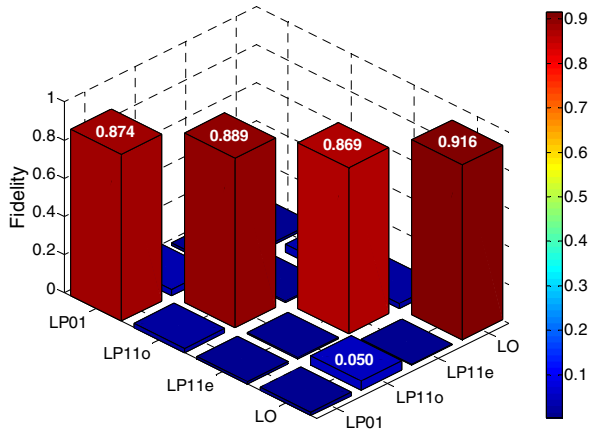


**Fig. 4.** Cross-correlation matrix of the normalized output field to ideal output field for different inputs. The four diagonal elements are the correlations of the $LP_{01}$ mode, $LP_{11o}$ mode, $LP_{11e}$ mode, and the LO.

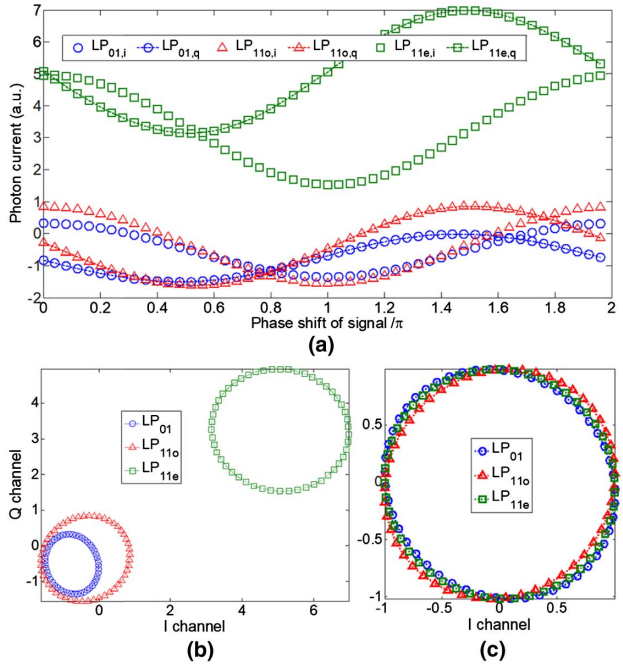


**Fig. 5.** (a) Photocurrent with balanced detection as a function of the phase shift of the input mode; in-phase versus quadrature components of the photocurrents (b) before and (c) after DC offset removal and amplitude rescaling.

**Table 1. Amplitude, Offset of Balance Detected Photocurrent, and Phase Error between the In-Phase and Quadrature Components**

| Mode | Amplitude of In-Phase | Amplitude of Quadrature | Offset of In-Phase | Offset of Quadrature | Phase Error |
|---|---|---|---|---|---|
| $LP_{01}$ | 0.75 | 0.84 | −0.75 | −0.50 | −5.86 |
| $LP_{11o}$ | 1.24 | 1.20 | −0.37 | −0.34 | 4.56 |
| $LP_{11e}$ | 1.92 | 1.71 | 5.06 | 3.27 | −2.21 |

**Table 2. Performance Metrics of Mode Demultiplexer and Optical 90-deg Hybrid**

| Mode | $LP_{01}$ | $LP_{11o}$ | $LP_{11e}$ | LO | Products |
|---|---|---|---|---|---|
| IL (dB) | −1.17 | −1.02 | −1.22 | −0.76 | −1.5–−1.0 |
| Xtalk (dB) | −14.74 | −13.95 | −15.89 | −13.03 | — |
| $\Delta IL_k$ (dB) | 0.75 | 0.74 | 1.33 | 2.62 | 0.5–2.0 |
| $\Delta\theta_k$ (deg) | 1.31 | −0.03 | 0.49 | 2.89 | 5 |
| Δdual (dB) | 0.50 | 0.15 | 0.49 | — | 0.2–1.0 |
| $\Delta\varphi$ (deg) | −5.86 | 4.56 | −2.21 | — | — |

offset resulting from the unequal power splitting (unequal spot amplitude in Fig. 3) of the LO. We plot the in-phase component versus the quadrature component in Fig. 5(b). They are approximately circles with offset centers. After the DC offset removal and amplitude rescaling, the three circles are almost overlapped in Fig. 5(c). The residual distortion is the phase error (in deg) between the in-phase and quadrature components defined as follows:

$$\Delta\varphi = \arcsin\left[\int_0^{2\pi} \overline{I}_i(\varphi)\overline{I}_q(\varphi)\mathrm{d}\varphi/\pi\right], \tag{8}$$

where $\overline{I}_{i,q}$ are the normalized photocurrents with the DC offsets removed. Note that the phase error defined here is a product of both the LO and signal phase retardation deviation in Eqs. (5) and (6) generated by the MDH. We summarize our findings in Table 1.

The ratio of the in-phase and quadrature amplitudes, also called the dual uniformity [24], has been used to evaluate the amplitude difference between the two quadrature components. The maximum dual uniformity of the three modes is 0.5 dB, which is comparable to that of commercial single-mode 90-deg hybrids.

We summarize the performance metrics of the MDH in Table 2. Compared with commercial single-mode 90-deg hybrids [24–26], the performance is comparable.

Increasing the number of phase plates can improve the performance. Figure 6 shows the IL, MDL, root mean square (RMS) of phase deviation ($\Delta\theta_k$), and intra-port power uniformity ($IL_k$) as a function of the number of phase plates. The IL and MDL gradually decrease as more phase plates are added. The reduction of phase error is minor when the number of phase plates is larger than four, similarly for intra-port power uniformity. More phase plates also add extra loss due to reflection, which is not considered in our model. Thus, we set four phase plates in our simulation.

The MDH also has a broad bandwidth. Within a 100-nm (1500–1600 nm) wavelength range, the variations in IL, MDL, and coupling efficiency are all less than 1.2 dB; the maximum intra-port power uniformity is smaller than 1 dB for both the signal and LO; and the phase error is smaller than 9 deg with four phase plates as shown in Fig. 7.

## 4. DISCUSSION

The results above show that MDHs can be realized with MPLC. In this section, we discuss some factors to consider in MDH design for experimental verification. They are phase retardation resolution of the phase plates, pixel size of the phase plates, MDH power loss, output beam coupling, and WDM application.

### A. Phase Retardation Resolution

The results above are obtained using phase plates with infinitesimal phase retardation resolution. However, it is impossible to fabricate a phase plate with infinitesimal resolution. In reality, limited by fabrication capabilities, the phase retardation is

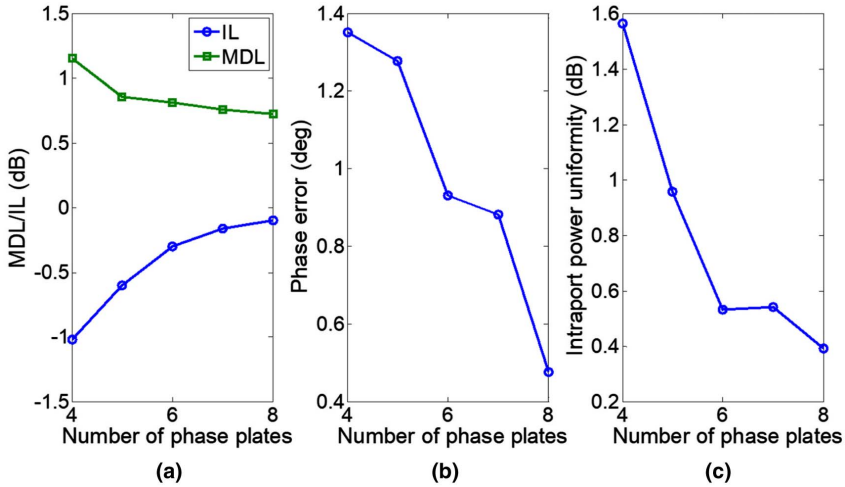


**Fig. 6.** Performance of a three-mode MDH as a function of the number of phase plates. (a) Insertion loss and mode-dependent loss, (b) phase deviation, and (c) intra-port power uniformity.

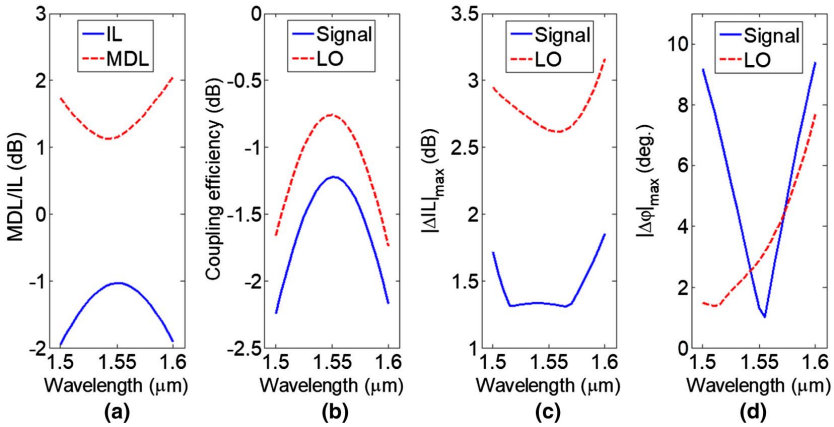


**Fig. 7.** (a) The IL and MDL, (b) power coupling efficiency, (c) the maximum intra-port power uniformity, and (d) the maximum absolute phase error as a function of the operating wavelength ranging from 1.5 to 1.6 μm, respectively.

discrete with finite resolution. The effect of finite phase retardation resolution ranging from 2 to 8 bits, corresponding to 90 and 1.4 deg, respectively, on the performance of MDHs, is shown in Fig. 8. The performance in terms of IL, MDL, coupling efficiency, the maximum intra-port power uniformity, and the maximum absolute phase error degrades notably if the resolution is lower than 4 bits, corresponding to 22.5 deg. This means that the MDHs allow smaller than 1/16 wavelength fabrication error for the phase plates.

### B. Pixel Size and Density

There exists a trade-off between performance and fabrication cost. Pixel size should be small enough to ensure the required resolution and diffraction. Generally, the pixel size should be a few times the wavelength, and at least 10 pixels must fit in the smallest beam diameter. However, too-small pixels should be avoided because of increased difficulty and cost in fabrication and alignment. Regarding size, the phase plate should be large enough to capture most of incoming beam and thereby reduce diffraction loss, but oversized phase plates waste unused space. The ratio between phase plate and pixel size determines the required pixel density. Figure 9 shows that the performance of the designed MDH varies less than 1 dB or 2 deg when the pixel size is increased from 3.4 to 17 μm. In the calculation, we fixed the size of the phase plate to 1367 μm, corresponding to pixel densities ranging from 401 × 401 to 81 × 81. The results show that the performance of MDHs is stable for large variations in pixel size.

### C. Power Loss

The dominant power loss in MPLC-based devices is from the surface reflection of phase plates (and mirrors in a reflective cavity configuration) when the phase plate is large enough to capture diffracted light. The reflection loss for each phase plate is twice the reflection loss of a single surface. For phase plates on a silica substrate without/with anti-reflection coatings, the single surface reflection losses are 4%/0.2%, respectively, corresponding to 0.35 dB/0.02 dB loss per phase plate, respectively. If the MPLC-based device is in a reflective cavity configuration, the reflection loss of the mirror/substrate of phase plates also has to be considered, about 0.04 dB per reflection for the best protected silver coated type. Another loss in MPLC

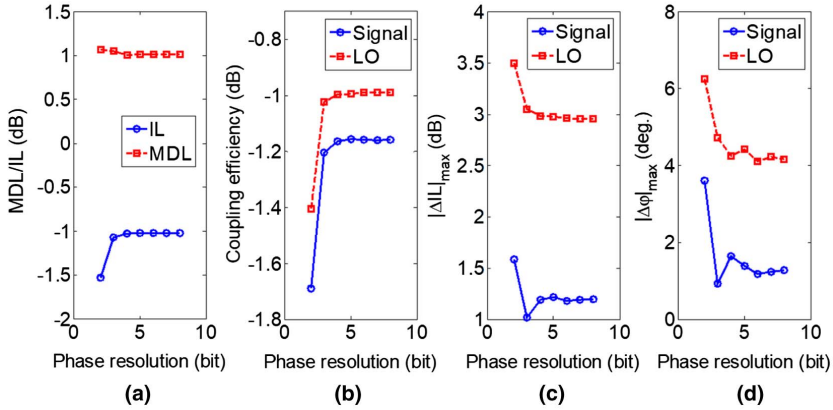


**Fig. 8.** MDH performance at phase retardation resolution of the phase plates from 2 to 8 bits. (a) The IL and MDL, (b) power coupling efficiency, (c) the maximum intra-port power uniformity, and (d) the maximum absolute phase error.

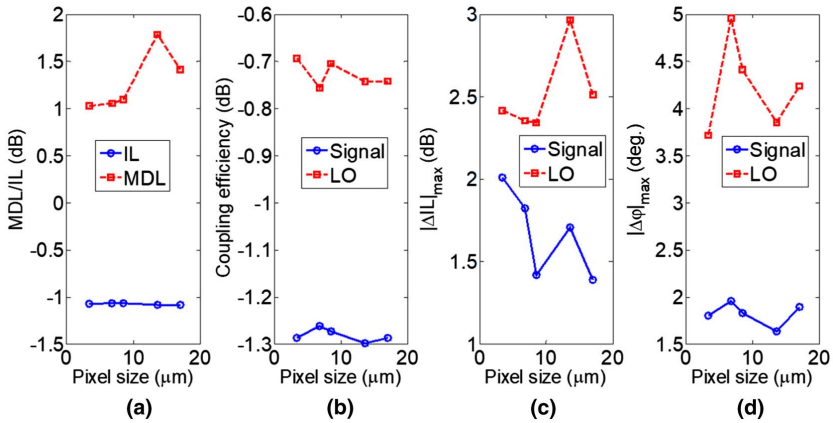


**Fig. 9.** MDH performance at different pixel sizes. (a) The IL and MDL, (b) power coupling efficiency, (c) the maximum intra-port power uniformity, and (d) the maximum absolute phase error.

devices is the coupling loss due to imperfect mode conversion, which induces mode mismatch between the output field and guided modes of a coupling fiber. The coupling loss is 1–3 dB in most cases and can be reduced by using more phase plates for better mode conversion, but at the cost of increased reflection loss. A trade-off between these two kinds of loss exists in practical applications.

### D. Output Beam Coupling

There are two options for coupling output beam from an MDH. The first one is coupling light of each spot into a pigtail of a photodetector. This approach requires spot spacing for the MDH output as large as hundreds of micrometers, resulting in a large required phase plate area. The coupling becomes laborious for a large quantity of modes. Since the outputs of an MDH are in a plane, they can be detected by directly shining photodetectors in a two-dimensional array [27] without coupling into the fiber. With properly designed parameters, output spots match the photodetector array in terms of pitch and mode field diameter that simplifies the coupling significantly. Besides, the photodetector pitch in two-dimensional arrays is as small as tens of micrometers, allowing for small spot spacing and making the MDH compact.

### E. WDM Application

An MDH can also be used to reduce device counts in WDM-overlaid MDM systems. In this system, $4M$ wavelength demultiplexers are connected to the outputs of the MDH for wavelength demultiplexing. The outputs of the wavelength demultiplexers are photodetected. One more WDM is needed to multiplex the LOs at different wavelengths before mixing. In this configuration, the total number of devices and connections is $4M + 2$ and $4MN + 4M + N + 1$, respectively, where $N$ is the number of wavelengths. By contrast, a traditional optical coherent receiver for MDM uses one mode demultiplexer, $M$ WDM demultiplexers, $MN$ optical 90-deg hybrids, and $N$ 1-to-$M$ power splitters (for shared LO). The total number of devices and connections in a traditional coherent receiver is $(M + 1)(N + 1)$ and $6MN + M + N$, respectively. The MDH simplifies the system dramatically if $N$ is larger than 4.

## 5. CONCLUSION

An optical front end for coherent receivers in SDM is proposed and demonstrated. The front end features multiple functionalities such as mode demultiplexing, optical 90-deg hybrid, and power splitting of the local oscillator, with a simple structure and no need for phase stabilization control. The proposed device can reduce the number of devices and power consumption in an SDM coherent receiver compared to the current optical front end. The concept of MDH is applicable not only to MDM but also to multicore fiber systems, where the mode demultiplexer is replaced by a fan-out device, and it can further be generalized to core- and mode-multiplexed systems using few-mode multicore fibers, where a fan-out together with mode demultiplexers is used.

**Funding.** Army Research Office (ARO) (W911NF1710500, W911NF1710553).

## REFERENCES

1. R.-J. Essiambre, G. J. Foschini, G. Kramer, and P. J. Winzer, "Capacity limits of information transport in fiber-optic networks," Phys. Rev. Lett. **101**, 163901 (2008).
2. D. J. Richardson, "Filling the light pipe," Science **330**, 327–328 (2010).
3. A. Chralyvy, "Plenary paper: the coming capacity crunch," in *35th European Conference on Optical Communication* (IEEE, 2009), p. 1.
4. P. J. Winzer, "Energy-efficient optical transport capacity scaling through spatial multiplexing," IEEE Photon. Technol. Lett. **23**, 851–853 (2011).
5. R. Ryf, S. Randel, A. H. Gnauck, C. Bolle, R.-J. Essiambre, P. Winzer, D. W. Peckham, A. McCurdy, and R. Lingle, "Space-division multiplexing over 10 km of three-mode fiber using coherent 6 × 6 MIMO processing," in *National Fiber Optic Engineers Conference* (Optical Society of America, 2011), paper PDPB10.
6. E. Ip, M.-J. Li, K. Bennett, Y.-K. Huang, A. Tanaka, A. Korolev, K. Koreshkov, W. Wood, E. Mateo, and J. Hu, "146$\lambda$ × 6 × 19-Gbaud wavelength-and mode-division multiplexed transmission over 10 × 50-km spans of few-mode fiber with a gain-equalized few-mode EDFA," J. Lightwave Technol. **32**, 790–797 (2014).
7. D. Richardson, J. Fini, and L. Nelson, "Space-division multiplexing in optical fibres," Nat. Photonics **7**, 354–362 (2013).
8. G. Li, N. Bai, N. Zhao, and C. Xia, "Space-division multiplexing: the next frontier in optical communication," Adv. Opt. Photon. **6**, 413–487 (2014).

9. H. Wen, C. Xia, A. M. Velázquez-Benítez, N. Chand, J. E. Antonio-Lopez, B. Huang, H. Liu, H. Zheng, P. Sillard, and X. Liu, "First demonstration of six-mode PON achieving a record gain of 4 dB in upstream transmission loss budget," J. Lightwave Technol. **34**, 1990–1996 (2016).
10. J. Luo, J. Li, Q. Sui, Z. Li, and C. Lu, "40 Gb/s mode-division multiplexed DD-OFDM transmission over standard multi-mode fiber," IEEE Photon. J. **8**, 7905207 (2016).
11. Y. Tian, J. Li, Z. Wu, Y. Chen, P. Zhu, R. Tang, Q. Mo, Y. He, and Z. Chen, "Wavelength-interleaved MDM-WDM transmission over weakly-coupled FMF," Opt. Express **25**, 16603–16617 (2017).
12. Y. Kokubun and M. Koshiba, "Novel multi-core fibers for mode division multiplexing: proposal and design principle," IEICE Electron. Express **6**, 522–528 (2009).
13. H. Liu, H. Wen, J. C. A. Zacarias, J. E. Antonio-Lopez, N. Wang, P. Sillard, A. A. Correa, R. Amezcua-Correa, and G. Li, "3 × 10 Gb/s mode group-multiplexed transmission over a 20 km few-mode fiber using photonic lanterns," in *Optical Fiber Communication Conference*, OSA Technical Digest (Optical Society of America, 2017), paper M2D.5.
14. E. Ip, A. P. T. Lau, D. J. F. Barros, and J. M. Kahn, "Coherent detection in optical fiber systems," Opt. Express **16**, 753–791 (2008).
15. S. Randel, R. Ryf, A. Sierra, P. J. Winzer, A. H. Gnauck, C. A. Bolle, R.-J. Essiambre, D. W. Peckham, A. McCurdy, and R. Lingle, "6 × 56-Gb/s mode-division multiplexed transmission over 33-km few-mode fiber enabled by 6 × 6 MIMO equalization," Opt. Express **19**, 16697–16707 (2011).
16. E. Ip, N. Bai, Y. K. Huang, E. Mateo, F. Yaman, M. J. Li, S. Bickham, S. Ten, J. Liñares, C. Montero, V. Moreno, X. Prieto, V. Tse, K. M. Chung, A. Lau, H. Y. Tam, C. Lu, Y. Luo, G. D. Peng, and G. Li, "88 × 3 × 112-Gb/s WDM transmission over 50 km of three-mode fiber with inline few mode fiber amplifier," in *37th European Conference and Exposition on Optical Communications*, OSA Technical Digest (Optical Society of America, 2011), paper Th.13.C.12.
17. R. Kunkel, H. Bach, D. Hoffmann, C. M. Weinert, I. Molina-Fernandez, and R. Halir, "First monolithic InP-based 90°-hybrid OEIC comprising balanced detectors for 100GE coherent frontends," in *IEEE International Conference on Indium Phosphide & Related Materials* (2009), pp. 167–170.
18. M. Seimetz and C. Weinert, "Options, feasibility, and availability of 2 × 4 90° hybrids for coherent optical systems," J. Lightwave Technol. **24**, 1317–1322 (2006).
19. J.-F. Morizur, L. Nicholls, P. Jian, S. Armstrong, N. Treps, B. Hage, M. Hsu, W. Bowen, J. Janousek, and H.-A. Bachor, "Programmable unitary spatial mode manipulation," J. Opt. Soc. Am. A **27**, 2524–2531 (2010).
20. G. Labroille, B. Denolle, P. Jian, P. Genevaux, N. Treps, and J.-F. Morizur, "Efficient and mode selective spatial mode multiplexer based on multi-plane light conversion," Opt. Express **22**, 15599–15607 (2014).
21. N. K. Fontaine, R. Ryf, H. Chen, D. T. Neilson, K. Kim, and J. Carpenter, "Scalable mode sorter supporting 210 Hermite-Gaussian modes," in *Optical Fiber Communications Conference and Exposition*, (Optical Society of America, 2018), paper Th4B.4.
22. T. J. Suleski and D. C. O'shea, "Gray-scale masks for diffractive-optics fabrication: I. Commercialslide imagers," Appl. Opt. **34**, 7507–7517 (1995).
23. Y. Sakamaki, T. Saida, T. Hashimoto, and H. Takahashi, "New optical waveguide design based on wavefront matching method," J. Lightwave Technol. **25**, 3511–3518 (2007).
24. Kylia, "90° optical hybrids COH," http://kylia.com/kylia/wp-content/uploads/2015/02/datasheet-COH-V1.2.pdf.
25. Optoplex, "90° optical hybrid," http://www.optoplex.com/download/Optical_Hybrid_ar.pdf.
26. Finisar, "High bandwidth integrated coherent receiver CPRV4220A," https://www.xsoptix.com/data/finisar/ds_fnsr_comp_CPRV4220A.pdf.
27. T. Umezawa, T. Sakamoto, A. Kanno, K. Akahane, A. Matsumoto, N. Yamamoto, and T. Kawanishi, "High-speed two-dimensional photodetector array for 4-WDM 25-Gbaud FSO communication," in *Optical Fiber Communication Conference*, OSA Technical Digest (Optical Society of America, 2018), paper M3K.7.